Electrochemical and Solid-State Letters, **6** (9) A194-A197 (2003)
0013-4651/2003/6(9)/A194/4/$7.00 © The Electrochemical Society, Inc.

Highly Reversible Lithium Storage in Nanostructured Silicon

J. Graetz,*,z C. C. Ahn, R. Yazami, and B. Fultz****

Division of Engineering and Applied Science, California Institute of Technology, Pasadena, California 91125, USA

Anode materials of nanostructured silicon have been prepared by physical vapor deposition and characterized using electrochemical methods. The electrodes were prepared in thin-film form as nanocrystalline particles (12 nm mean diameter) and as continuous amorphous thin films (100 nm thick). The nanocrystalline silicon exhibited specific capacities of around 1100 mAh/g with a 50% capacity retention after 50 cycles. The amorphous thin-film electrodes exhibited initial capacities of 3500 mAh/g with a stable capacity of 2000 mAh/g over 50 cycles. We suggest that the nanoscale dimensions of the silicon circumvents conventional mechanisms of mechanical deterioration, permitting good cycle life.
 [DOI: 10.1149/1.1596917]

Manuscript submitted February 7, 2003; revised manuscript received April 19, 2003. Available electronically July 3, 2003.

There is intense interest in developing new materials for anodes and cathodes that store higher densities of lithium. From the criterion of lithium density, the ultimate anode would be lithium metal itself. Unfortunately, issues of safety have confined lithium anodes to small rechargeable cells. During charging, lithium metal is electroplated onto the anode surface, but there is no thermodynamic tendency to stop the formation of shape asperities such as dendrites that can cause short circuits across the electrolyte.[1] A framework material seems necessary for preserving the anode shape, and metallic alloys can provide this function. The Li-Si system has the potential for one of the highest gravimetric capacities. Electrochemical alloying of lithium with silicon to form alloys of Li_xSi has shown stable crystalline phases up to $Li_{4.4}Si$.[2-6] For a range of x from 0 to 4.4 the theoretical specific capacity of pure silicon is 4200 mAh/g, far greater than the theoretical capacity of 372 mAh/g for graphitic carbons. Furthermore, lithium alloys do not suffer from the solvent cointercalation that can occur in graphitic carbons, and may degrade the storage capacity.[7-11] These advantages of silicon anodes are well known, but it is also well known that a 300% volume dilatation is associated with alloying 4.4 lithium atoms per silicon atom. This generates enormous mechanical stresses within the brittle material, which pulverizes during the first few charge/discharge cycles and electrical integrity is lost.[11-14] Li *et al.* have recently shown that bulk silicon loses approximately 90% of its initial capacity after five cycles at ambient temperature.[15]

The properties of nanostructured materials have also received intense interest over the last decade. When dimensions in a material are tens of nanometers, the conventional mechanisms for deformation and fracture are expected to be altered. There is some evidence that thin films of silicon (1.2 μm) prepared by chemical vapor deposition undergo smaller capacity losses during cycling than bulk silicon.[14] Sayama *et al.* have shown discharge capacities of up to 4000 mAh/g over 10 cycles in chemical vapor deposition (CVD) silicon electrodes.[16] Evaporated thin films (40 nm) have shown stable capacities of up to 3000 mAh/g over 25 cycles.[17] Similarly, small silicon particles (80 nm) have shown capacities near 1700 mAh/g on the tenth cycle.[15] In this case, the improved cycling performance was achieved with 10-40 wt % of binders and conductive additives. These additions degrade significantly both the gravimetric and volumetric capacities of the electrode. In this work we used direct depositions of nanomaterials onto a metallic current collector without the use of conductive additives or binders. The electrodes were intentionally made very thin so that the intrinsic properties of nanostructured materials could be measured. We report a promising capacity for charge/discharge cycling of two types of nanostructured silicon anodes, and we suggest that the good cycle life of these materials originates with the unique micromechanics of nanostructured materials.

Experimental

Our nanostructured electrode materials were prepared by two different processes, and have different nanostructures. In the first process, nanocrystalline silicon clusters were prepared by gas-phase condensation and ballistic consolidation on planar copper current collectors. A mixture of 90% N_2 and 10% H_2 was used as a ''forming gas'' at a pressure differential of 2 Torr. The elemental silicon charge was heated in a tungsten wire basket and evaporated into the gaseous atmosphere. In the gas, the silicon atoms are cooled rapidly, and nanocrystals are nucleated as the atoms collide. The nanocrystals move by Brownian motion in the gas, forming loose agglomerates when they meet. These particles, entrained in the gas, approach the sound velocity as the gas is drawn through a nozzle. The particles form a thin film of ballistically consolidated nanocrystals when they hit the substrate at high speed.

In the second process, nanostructured films of silicon were prepared by evaporation onto planar nickel current collectors. A charge of elemental silicon was heated in a tungsten wire heating basket, and evaporated under a vacuum of 6×10^{-6} Torr. The nickel substrate was placed directly below the tungsten basket, and the evaporated silicon atoms were deposited on the substrates in a continuous thin film of approximately 100 nm in thickness.

The structures of the materials are shown in the transmission electron microscopy (TEM) micrographs of Fig. 1. In the ballistically deposited electrode, the silicon nanocrystals form a web of interconnected particles. A conventional and a high-resolution bright-field image and the associated electron diffraction pattern of the as-deposited nanocrystalline silicon are shown in Fig. 1a, b. The most obvious features of these images are the small crystallites (5-20 nm in diameter) and the low density of the material. For the evaporated thin films, the absence of sharp peaks in the electron diffraction patterns (inset of Fig. 1c) shows that the material is entirely amorphous. The absence of long-range order was confirmed by X-ray diffractometry. The lack of structure in the bright-field image in Fig. 1c indicates a uniform film unbroken by grain boundaries, dislocations, or cracks. Figure 1d shows a TEM cross-sectional image of the evaporated silicon, showing it to be 100 nm thick.

Electrochemical tests were performed using a metallic lithium counter electrode in a stainless steel 2016 coin cell. Approximately 50 μg of silicon was used in the electrochemical cells. The electrode mass was determined using TEM and a Metler microbalance sensitive to 1 μg. A 0.50 mm thick fiberglass separator was used to isolate the silicon cathode from the lithium anode. A mixture of ethylene carbonate and dimethyl carbonate (EC DMC) with $LiPF_6$ (Mitsubishi Chemical Co.) was used as an electrolyte. All test cells were assembled in an argon atmosphere and cycled at a rate of C/4 using an Arbin Instruments BT2000 battery cycler.

* Electrochemical Society Student Member.
** Electrochemical Society Active Member.
z E-mail: graetz@caltech.edu

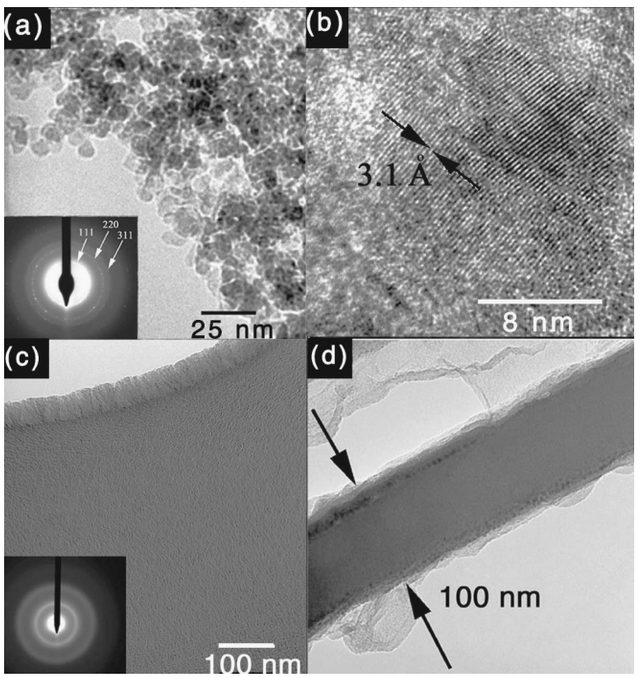

Figure 1. (a) Bright-field TEM image and electron diffraction pattern of ballistically deposited silicon showing interconnected nanocrystals. (b) A high-resolution TEM image of a silicon nanocrystal. (c) Bright-field planar view with associated electron diffraction pattern, and (d) TEM cross section from evaporated amorphous silicon showing the uniform, continuous nature of the as-deposited 100 nm film.

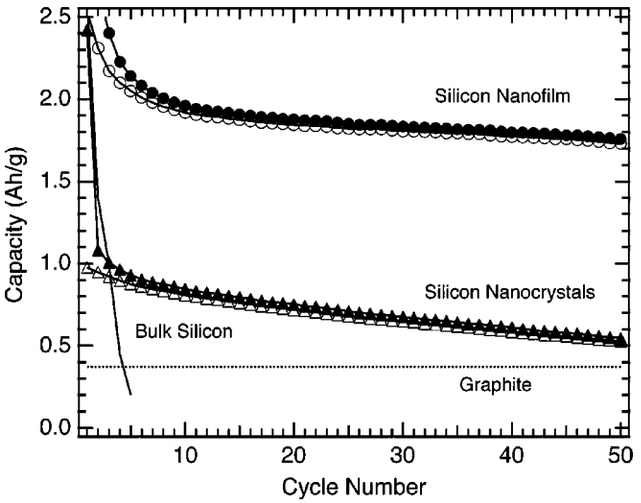

Figure 3. The gravimetric capacity of the ballistically deposited silicon nanocrystals and the evaporated silicon nanofilm over 50 cycles. For reference, the theoretical specific capacity of graphite (LiC_6) and the experimentally measured capacities for bulk silicon[15] are also included. The light and dark markers indicate the charge and discharge cycles, respectively.

Results and Discussion

The voltage profiles from electrochemical cycles 1, 2, 25, and 50 are shown in Fig. 2a for the ballistically consolidated nanocrystalline silicon. This figure shows an initial discharge capacity (Q_d) of 2400 mAh/g during the first insertion of lithium, and a subsequent charge capacity of 1000 mAh/g (Q_c), giving a coulombic efficiency (Q_c/Q_d) of 41% for the first cycle. This high irreversible capacity was limited to the first cycle, however. Cycles 2-50 show a mean specific capacity of 750 mAh/g (Fig. 3). The capacity fade correlates inversely with the coulombic efficiency, which increased steadily up to 96% by cycle no. 9. In this reversible region, the nanocrystalline

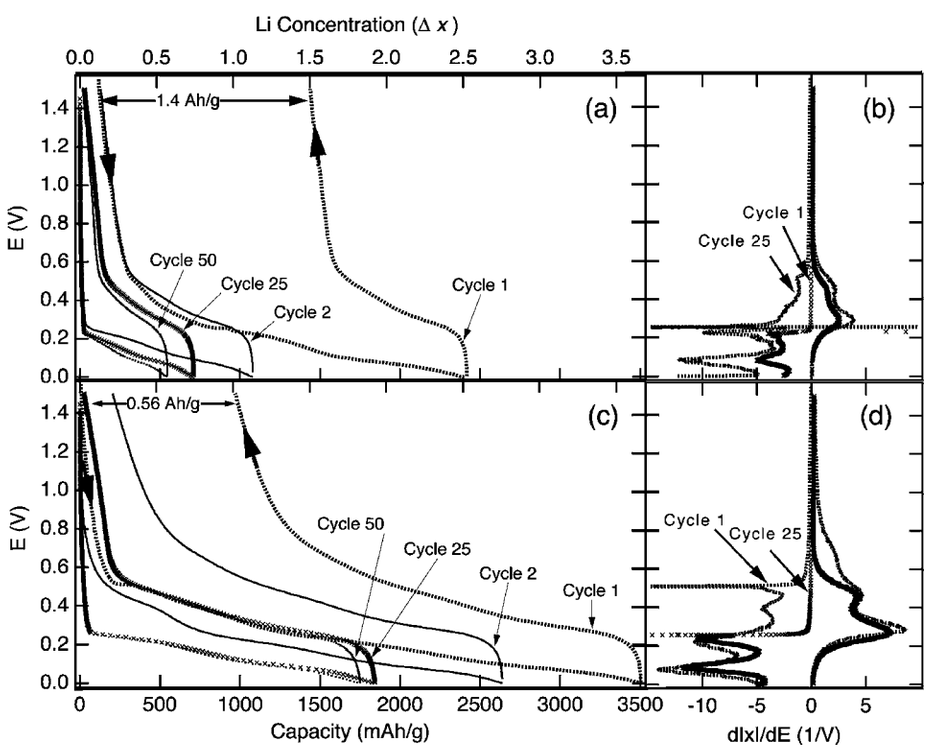

Figure 2. Voltage profile of cycles 1, 2, 25, and 50 from (a) the ballistically deposited silicon nanocrystals and (b) the differential capacity curves for cycles 1 and 25. (c) Voltage profile of cycles 1, 2, 25, and 50 from the evaporated amorphous silicon nanofilm and (d) the differential capacity curves for cycles 1 and 25. The arrows indicate the cycling direction for the first cycle. Here x denotes lithium concentration, as in Li_xSi.

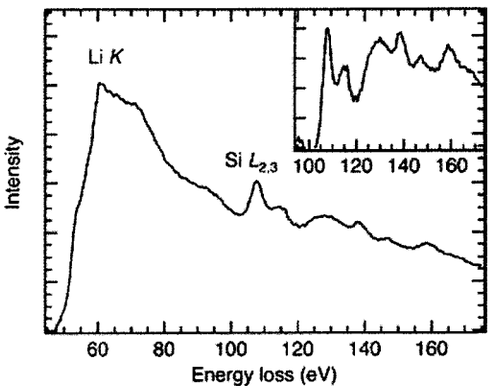

Figure 4. Background-subtracted Li K edge from the fully lithiated silicon nanocrystals after the first discharge. The inset shows the background subtracted Si $L_{2,3}$ edge. Quantitative analysis of these edges yields an atomic ratio (N_{Li}/N_{Si}) of 4.3.

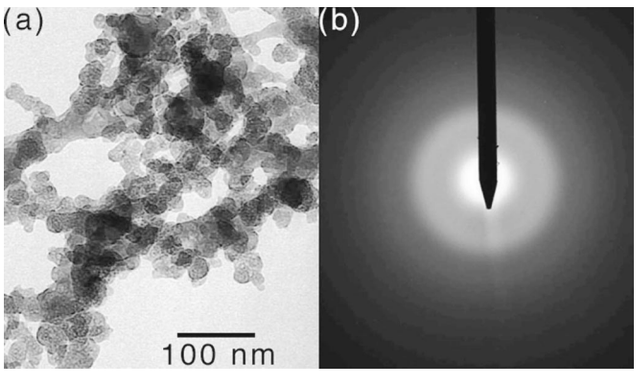

Figure 5. TEM of silicon electrode after the first discharge (fully lithiated) showing (a) a bright-field image and (b) an electron diffraction pattern with broad amorphous rings.

electrode exhibited a mean capacity loss of approximately 20 mAh/g per cycle with a final capacity of 525 mAh/g on cycle number 50.

An elemental analysis of the fully lithiated ballistically consolidated silicon was performed using quantitative electron energy-loss spectroscopy (EELS). The energy-loss spectrum in Fig. 4 clearly shows a strong lithium K edge at around 54 eV. The edge intensity was determined using a 20 eV integration window about the lithium K edge (55-75 eV) and silicon $L_{2,3}$ edge (99-119 eV). An atomic ratio was calculated using the ratio of the edge intensities weighted by the hydrogenic cross sections.[18] The quantitative EELS analysis revealed an atomic ratio N_{Li}/N_{Si} as large as 4.3 after the first discharge. This suggests that the lithiated stoichiometry is close to that of the $Li_{22}Si_5$ phase, and confirms that the lithium is not simply plated on the surface but is actually inserted into the silicon host.

Even better electrochemical performance was found for the thin amorphous films. The voltage profiles obtained from cycles 1, 2, 25, and 50 are shown in Fig. 2c. The initial discharge capacity of ~3500 mAh/g suggests that up to 3.6 lithium atoms per silicon atom are involved in the initial alloying. The subsequent charge capacity of 2500 mAh/g (2.6 lithiums per silicon atom) yields a coulombic efficiency of 71% on the first cycle. Upon subsequent cycling, the electrode exhibited a stable specific capacity around 1800 mAh/g (Fig. 3). The capacity stabilization corresponds to an increase in the coulombic efficiency to 98% on cycle no. 9. After 20 cycles, the amorphous thin film exhibited a mean capacity loss of only 8 mAh/g per cycle.

The low coulombic efficiencies of the first cycles can be attributed in part to the formation of a solid-electrolyte interphase (SEI). This passivation layer is expected to form through a reaction of the lithium with the solvent (EC DMC) and the salts ($LiPF_6$) of the electrolyte. The formation of an SEI leads to an irreversible capacity through two mechanisms, the loss of lithium to the formation of the SEI and an increase in the cell impedance. Because the sharp capacity fade is limited to the first few cycles, we believe that the reactions contributing to the SEI layer occur during the initial cycles. The SEI formation is supported by the 500 mV peaks in the differential capacity plots of Fig. 2b and d, which disappear after a few cycles. The SEI formation was further confirmed with scanning electron microscopy, which clearly showed a smooth passivation layer on the electrode surface after the initial lithiation. Other surface contaminants include a native oxide, which was observed with transmission EELS. It is thermodynamically favorable for lithium to reduce SiO_2. It is likely that the large quantity of SiO_2 in the high-surface area nanocrystals is partially responsible for the higher first cycle irreversible capacity in the nanocrystalline electrode. The overall reduced capacity of this electrode is also attributed to the high concentration of SiO_2 present as a surface oxide. After cycle no. 20 or so, we believe the capacity fade originates with the spallation of silicon from the metal contact because such particles were found in the cell after extensive cycling. For the nanocrystalline silicon this later-stage capacity fade depended on the type and preparation of the substrate surface, although this was not investigated systematically.

Compared to bulk silicon, which has essentially no cycle life, both types of nanostructured silicon have far superior performance during charge/discharge cycling. The improved cycle life is achieved by eliminating the particle decrepitation. Figure 5a shows a TEM image of the fully lithiated ballistically deposited particles, which clearly shows that the individual nanoparticles and the loose agglomerates of Fig. 1a are still intact. The lack of cracks or broken particles is attributable to the absence of conventional mechanisms for microstructural damage. Dislocations have never been reported in crystals with dimensions of those considered in this study ($<$20 nm), probably because any such dislocations are quickly drawn to the surface by image forces. For brittle materials such as silicon, decrepitation occurs through the formation of cracks and their propagation by dislocation emission from the crack tip. For a crack to propagate, however, it must exceed a critical size, a_c

$$a_c = \frac{2}{\pi}\frac{K_{1c}^2}{\sigma^2} \qquad [1]$$

The fracture toughness, K_{1c}, and yield strength, σ, in polycrystalline silicon are approximately 0.751 MPa/m$^{1/2}$ [19] and 1.1 GPa,[20] respectively. These values yield a critical flaw size of around 300 nm, much larger than the dimensions of our nanostructured electrode materials. Although this calculation is for pure silicon, the critical flaw size of lithiated silicon is not expected to be comparable to the dimensions of our films, which are nearly an order of magnitude smaller.

Gradients in strain can cause defect generation in solids, so gradients of lithium concentration could cause microstructural damage in bulk silicon. An advantage of nanostructured materials is that their relaxation times, τ, for diffusion are short, owing to their small dimensions, d, since $\tau = d^2/D$, where D is the diffusivity. Therefore, strains due to alloying and diffusion dissipate much more quickly in nanostructured materials. The lithium concentration is more uniform across nanostructured materials cycled at moderate rates.

The absence of flat plateaus in the reversible voltage profiles of Fig. 2a and c suggest that the evaporated film and the nanocrystalline electrodes are amorphous during cycling and do not form stoichiometric compounds. This is not surprising because crystalline silicon forms a metastable glassy phase upon lithiation at room temperature.[21] The transformation of crystalline silicon into an amorphous lithium alloy is confirmed by the broad amorphous rings

of the electron diffraction pattern in Fig. 5b. By avoiding crystallographic phase changes these materials considerably suppress local stress gradients due to electrochemical alloying.

The relatively open structure of the ballistically consolidated nanocrystalline silicon material seems capable of accommodating the large volume expansions of lithiation. It is more difficult to understand why the amorphous silicon nanofilms were even more robust during electrochemical cycling. It is expected that the volume expansion in the thin film would lead to the decohesion of the film from its metal substrate. It is plausible, however, that the film is separated from the substrate along much of its interface, making electrical contact at a few points. Perhaps the film bows outward during lithiation, but remains anchored adequately for electrical continuity.

Conclusion

The reversible capacities of nanostructured silicon films were as high as 2000 mAh/g, and stable over 50 cycles. The high capacity is expected from the phase diagram of the Li-Si system, but the cycle life depends on the nanostructured nature of the materials. The improved cycling of nanostructured silicon are attributed to the dimensions of these materials, which are too small to permit the bulk micromechanical processes of deformation and fracture.

Acknowledgments

This work was supported by the Department of Energy through Basic Energy Sciences grant no. DE-FG03-00ER15035. We thank Crane & Co., Inc. for providing the fiberglass used as a separator in the electrochemical cells.

California Institute of Technology assisted in meeting the publication costs of this article.

References

1. J. Yamaki and S. Tobishima, *Handbook of Battery Materials*, p. 339, Wiley-VCH, New York (1999).
2. R. A. Sharma and R. N. Seefurth, *J. Electrochem. Soc.*, **123**, 1763 (1976).
3. C. J. Wen and R. A. Huggins, *J. Solid State Chem.*, **37**, 271 (1981).
4. C. van der Marel, G. J. B. Vinke, and W. van der Lugt, *Solid State Commun.*, **54**, 917 (1985).
5. R. Nesper and H. G. V. Schnering, *J. Solid State Chem.*, **70**, 48 (1987).
6. W. J. Weydanz, M. Wohlfahrt-Mehrens, and R. A. Huggins, *J. Power Sources*, **81**, 237 (1999).
7. J. O. Besenhard and H. P. Fritz, *J. Electrochem. Soc.*, **53**, 329 (1974).
8. J. O. Besenhard, *Carbon*, **14**, 111 (1976).
9. J. O. Besenhard, J. Yang, and M. Winter, *J. Power Sources*, **68**, 87 (1997).
10. R. Yazami and S. Genies, *Denki Kagaku oyobi Kogyo Butsuri Kagaku*, **66**, 1293 (1998).
11. M. Winter, J. O. Besenhard, M. E. Spahr, and P. Novak, *Adv. Mater. (Weinheim, Ger.)*, **10**, 725 (1998).
12. J. Yang, M. Winter, and J. O. Besenhard, *Solid State Ionics*, **90**, 281 (1996).
13. M. Winter and J. O. Besenhard, *Electrochim. Acta*, **45**, 31 (1999).
14. S. Bourderau, T. Brousse, and D. M. Schleich, *J. Power Sources*, **81**, 233 (1999).
15. H. Li, X. Huang, L. Chen, Z. Wu, and Y. Liang, *Electrochem. Solid-State Lett.*, **2**, 547 (1999).
16. K. Sayama, H. Yagi, Y. Kato, S. Matsuta, H. Tarui, and S. Fujitani, Abstract 52, The 11th International Meeting on Lithium Batteries, Monterey, CA, June 23-28, 2002.
17. T. Takamura, S. Ohara, J. Suzuki, and K. Sekine, Abstract 257, The 11th International Meeting on Lithium Batteries, Monterey, CA, June 23-28, 2002.
18. R. F. Egerton, *Electron Energy Loss Spectrometry in the Electron Microscope*, Plenum, New York (1986).
19. C. P. Chen and M. M. Leipold, *Am. Ceram. Soc. Bull.*, **59**, 469 (1980).
20. J. Bagdahn and W. N. Sharpe, Jr., *Sens. Actuators A*, **103**, 9 (2003).
21. P. Limthongkul, Y. I. Jang, N. Dudney, and Y. M. Chiang, *Acta Mater.*, **51**, 1103 (2003).